RESEARCH PAPER

Improving the Mechanical and Thermal Characteristics of Epoxy by a Multi-Phase Nanocomposite (Epoxy/PSA/CF/SiO_2)

Ali Mohammadi Mehra [1], *Masood Hamadanian* [1,2] *

[1] *Institute of Nano Science and Nano Technology, University of Kashan, Kashan, I.R. Iran*

[2] *Department of Physical Chemistry, Faculty of Chemistry, University of Kashan, Kashan, I.R. Iran*

ARTICLE INFO

Article History:
Received 01 June 2025
Accepted 29 September 2025
Published 01 October 2025

Keywords:
Carbon fiber
Epoxy
Nanocomposite
Polystyrene acrylic
SiO_2 nanoparticle

ABSTRACT

In recent years, researchers have drawn attention to the fact that the mechanical properties of hybrid composite materials reinforced with carbon fibers and nanoparticles are significantly superior to those of conventional composites. This study investigates the use of epoxy nanocomposites reinforced with carbon fiber (CF), polystyrene acrylic (PSA, 0–2 wt%), and SiO_2 nanoparticles. To optimize the mechanical performance, response surface methodology (RSM) and central composite design were employed. The composites were characterized using various techniques such as FT-IR, XRD, SEM, EDX, and TGA, while tensile tests were conducted to evaluate their mechanical properties. The results revealed that the addition of CF, PSA, and SiO_2 significantly enhanced the stress, strength, and strain of the composites compared to neat epoxy. The optimal performance was achieved at 1.59 wt% CF, 1.29 wt% PSA, and 0.40 wt% SiO_2, confirming the synergistic role of these reinforcements in improving the mechanical and thermal behavior of the composites.

How to cite this article
Mehra A., Hamadanian M. Improving the Mechanical and Thermal Characteristics of Epoxy by a Multi-Phase Nanocomposite (Epoxy/PSA/CF/SiO_2). J Nanostruct, 2025; 15(4):1925-1944. DOI: 10.22052/JNS.2025.04.039

INTRODUCTION

Throughout human history, there has been a desire to combine materials in order to create new and improved materials with enhanced qualities and performance. This has led to the development of composite materials, which have been the focus of numerous endeavors. From the earliest straw and mud-based composites to the most modern carbon fiber composites used in spacecraft bodies, the creation of these materials has been a significant achievement. The main advantage of composites is their ability to combine the desired characteristics of their elements, resulting in materials with superior attributes [1]. The properties of composites, including physical, chemical, mechanical, and thermal properties, depend on factors such as the type of ingredients, percentage composition of components, shape and arrangement of reinforcing particles, and the connection of the two components [2]. Due to its strong mechanical properties, chemical resistance, high adhesion to various reinforcements, and cost-effective manufacturing, epoxy is commonly used as a matrix in polymer composites [3, 4]. Unfortunately, the network structure of these materials makes them brittle, resulting in low toughness and impact resistance. This is a major issue when using thermoset polymers [1-3]. Kevlar, glass, and carbon are commonly used fibres due to their low weight and high stiffness [5]. Carbon

* *Corresponding Author Email: hamadani@kashanu.ac.ir*

Fiber, with its distinct mechanical properties, is employed as a reinforcing phase in composites in various industries such as aerospace, military, and automotive. For example, in the aerospace industry, it is used to make lightweight and strong aircraft components [6].

Due to its outstanding properties, such as low density, high modulus, and high strength, as well as its resistance to high temperatures, chemical corrosion, and thermal expansion, carbon fiber reinforced epoxy resin (CFREP), also known as "black gold," is widely utilized in various industries in fields such as aerospace, automotive, and sports equipment [2, 3, 7, 8]. The performance of thermoset CFREPs has been enhanced through numerous studies. Some of these studies are focused on finding manufacturing and treatment techniques that can enhance the bond between the binder and the Fiber [9]. Some of these studies are focused on developing stronger epoxy materials. One approach to achieve this is by incorporating micro- and nano-additives into the matrix, which can improve the mechanical properties of carbon fiber reinforced polymers [10, 11]. Hybrid reinforced composites, also known as "hybrids," are a type of substance that has been gaining recognition for its potential in structural applications. These hybrids possess superior mechanical properties, chemical inertness, and thermal stability at very high temperatures, making them ideal for use in various industries. In particular, oxide nanoparticles such as Al_2O_3, TiO_2, SiO_2, and ZrO_2 have been identified as the most preferred candidates due to their low production cost compared to other types of oxide nanoparticles and carbon nanomaterials like carbon nanotubes [1].

Cho et al increased the longitudinal compressive strength of carbon/epoxy composites by 10% and 16% by adding 3% and 5% weight of graphite nanoparticles, respectively, into the resin with a volume fraction of 55% fiber [12]. He et al. analyzed the compressive strength of nano-calcium carbonate/epoxy and its fiber composites, showing a significant improvement of 13.5% and 14.1% in compressive strength for the cured bulk epoxy matrix and its fiber composites filled with 4 wt% nano-$CaCO_3$, respectively [13]. Sánchez et al. reported a significant increase in flexural strength with the addition of functionalized carbon nanotubes. Specifically, there was a 12% improvement in flexural strength at a CNT–NH_2 content of 0.3 wt.%. [14].

MATERIAL AND METHODS

Feedstock and chemicals

The supplier of epoxy resin was Kumho P&B Chemicals in Seoul, South Korea. The following are some of the usual properties of epoxy resin: a molar mass of 184–190, a viscosity of 12,000–14,000 mPa at 25°C, and a density of 1.16 g/cm³ at that temperature. The curing ingredient for the epoxy resin, cycloaliphatic amine (KH 816), was provided by Kukdo Chemical Industry Co., Ltd. in Qiandeng Town, China. Additionally, Parseshen Co., Ltd. supplied polystyrene acrylic (PSA) with a density of 0.86 g/cm³ at 25 °C in Tehran, Iran. Commercially available carbon fibers from Zoltek-USA were used as the reinforcing components for the fiber composites. The Kimia Tehran Acid Company provided us with a commercial white powder of sodium silicate with a density of 2.4 g/ cm³. This powder, composed of SiO_2, Na_2O, and H_2O, has weight% % 24.9, 20.9, and 54.2, respectively.

Synthesis of silica nanoparticles (SiO_2)

A gel was formed by adding diluted sodium silicate dropwise (2 drops/s) to 28 ml of 2.5% HCl and agitating at 250 rpm at 60°C until the gel was formed. We marked 7 mL of sodium silicate as the correct amount. The gel was then cleaned with distilled water until no Cl- ions remained. To test for the presence of Cl ions, a diluted silver nitrate solution (0.1 M) was applied to the filter. A white precipitate formed, indicating the presence of Cl

Table 1. Design matrix for central composite design.

Variables	Units	Symbol code	Low Level	High Level	-Alpha	+Alpha
SiO_2-Nanoparticles	wt%	A	0.41	1.59	0	2
Carbon Fiber	wt%	B	0.41	1.59	0	2
Polystyrene Acrylic	wt%	C	1.01	3.99	0	5

ions. The silver nitrate was added multiple times until no white precipitate developed. The gel was then dried in an oven at 100°C for 26 hours and calcined in air at 950°C for an hour [15].

Sodium silicate (Na_2SiO_3) is dissolved in water to form orthosilicic acid ($Si(OH)_4$), the simplest form of silica in solution. $Si(OH)_4$, a weak acid with a pKa of 9.8 (corresponding to a pH of approximately 4.5), consists of silicon in a tetrahedral coordination with four hydroxyl groups. At room temperature, $Si(OH)_4$ remains stable in water only when its concentration is below the solubility limit of the amorphous phase (typically around 100 ppm). At higher concentrations, $Si(OH)_4$ undergoes spontaneous polycondensation to reduce its concentration in solution, producing one water molecule per condensation reaction between two $Si(OH)_4$ molecules. Additionally, even at a pKa of 9.8, a small fraction (approximately 0.18%) of $Si(OH)_4$ molecules ionize at neutral pH. These ionized molecules rapidly react with neutral $Si(OH)_4$ molecules to form oligomers. This spontaneous condensation process initially generates a range of small oligomers, which serve as nuclei for the formation of stable particles. These nuclei eventually coalesce or aggregate to form a gel or an aggregated network, leading to the formation of silica nanoparticles.

Experimental Design

Response Surface Methodology (RSM) is a valuable approach for developing, enhancing, and optimizing process parameters. This experimental strategy is particularly useful for determining the optimal conditions in a multivariable system [16]. One benefit of using Central Composite Design (CCD) in experimental design for RMS is that it reduces the number of tests needed to analyze the interaction between different input variables. This design is particularly effective for both parameter interaction analysis and optimizing useful parameters with minimal experiments. In this approach, the independent variables were the weight percentages of SiO_2 NPs (A), carbon fiber (B), and polystyrene acrylic (C). Table 1 outlines the ranges and levels of these variables, as well as the levels of alpha. To model and optimize the material characteristics of the Epoxy/PSA/CF/SiO_2

Table 2. Experimental design matrix and mechanical properties results of Epoxy/PSA/CF/SiO_2 nanocomposite.

Std	Run	A (NPs)	B (CF)	C (PSA)	Stress	Strain	Area	Modulus	Yield
5	1	0.41	0.41	3.99	39.11	8.80	493.87	6.89	38.07
12	2	1.00	2.00	2.50	66.71	9.51	957.07	10.04	65.32
13	3	1.00	1.00	0.00	44.26	6.94	389.56	10.17	42.52
1	4	0.41	0.41	1.01	40.92	6.86	435.27	7.94	39.73
3	5	0.41	1.59	1.01	71.14	10.31	1055.85	10.74	69.25
11	6	1.00	0.00	2.50	30.28	9.47	487.79	4.02	26.45
4	7	1.59	1.59	1.01	57.14	9.23	810.13	9.68	55.85
10	8	2.00	1.00	2.50	55.25	9.98	770.17	8.92	53.88
7	9	0.41	1.59	3.99	51.80	10.05	658.48	8.73	50.48
19	10	1.00	1.00	2.50	49.81	9.44	672.16	8.62	48.76
16	11	1.00	1.00	2.50	53.26	9.26	747.85	8.44	51.94
18	12	1.00	1.00	2.50	48.12	8.01	562.32	8.79	46.62
14	13	1.00	1.00	5.00	56.27	8.04	712.50	9.46	54.84
8	14	1.59	1.59	3.99	46.11	8.94	646.89	8.47	44.65
9	15	0.00	1.00	2.50	53.87	11.55	781.06	8.71	52.31
2	16	1.59	0.41	1.01	35.40	8.13	490.68	6.17	34.32
20	17	1.00	1.00	2.50	45.36	8.24	620.53	7.90	44.34
17	18	1.00	1.00	2.50	55.31	9.02	780.38	8.79	54.16
15	19	1.00	1.00	2.50	52.65	8.50	713.91	8.81	51.67
6	20	1.59	0.41	3.99	37.27	8.30	469.29	6.43	36.20

nanocomposite, this study utilized Design Expert (version 13) software and employed RSM and central composite design (CCD).

Preparation of Epoxy/PSA/CF/SiO_2 Nanocomposite

To determine the necessary amount of epoxy for the silicone mold, the quantities of PSA, carbon fiber, and SiO_2 nanoparticles were calculated using the data from Table 2. The pre-weighed epoxy was then mixed with the required nanoparticles for 10 minutes using a magnetic stirrer. Next, the measured amount of PSA was added to the mixture and stirred for 30 minutes. The mixture was then sonicated for 15 minutes. Once the appropriate amount of hardener was added, the mixture was poured into the silicone mold along with the carbon fibers. Fig. 1 illustrates the schematic representation of the Epoxy/PSA/CF/SiO_2 nanocomposite preparation.

Characterization techniques

A Fourier Transform Infrared Spectrophotometer (Nicolet-Impact 400D) was used to examine the bonds created or broken by the alteration in the range of 400–4000 cm^{-1}. XRD was performed using a Philips X-pert Pro MPD model X-ray diffractometer with CuKα radiation (λ = 0.1540 nm) as the X-ray source in the range of 2Θ = 10°–80° for microstructural analysis. The morphology and cross-section of the silica nanoparticles and nanocomposites were analyzed using scanning electron microscopy (SEM, model S-4160, Hitachi, Japan) equipped with energy-dispersive spectroscopy (EDS) analysis (Peronis 2100, Japan). The thermographic examination of the nanocomposite samples was conducted using a TGA instrument (TG-DTA, BAHR STA 503 model, Germany) to determine the different stages of decomposition and degradation that occurred during the polymerization process. The introduced samples by the Design Expert software consisted of twenty projected standard and optimized samples were subjected to tensile tests using a 20KN universal testing machine model TB1. The tests were conducted on nanocomposites. These samples were loaded at a strain rate of 5 mm/min. Table 2 presents the final results of stress, strain, area, modulus, and yield for these nanocomposites.

RESULTS AND DISCUSSION

Characterization of silica nanoparticles

Fig. 2(a) shows the XRD pattern of SiO_2 nanoparticles, indicating a low-cristobalite type crystalline structure corresponding to the JCPDS number 01-076-0941 [17]. The Debby Scherrer formula was utilized to determine the average particle size of SiO_2 nanoparticles, which was found to be approximately 27nm.

In addition, the microstrain (ε) of the nanoparticles was evaluated using the Williamson-Hall method, which is based on the XRD peak

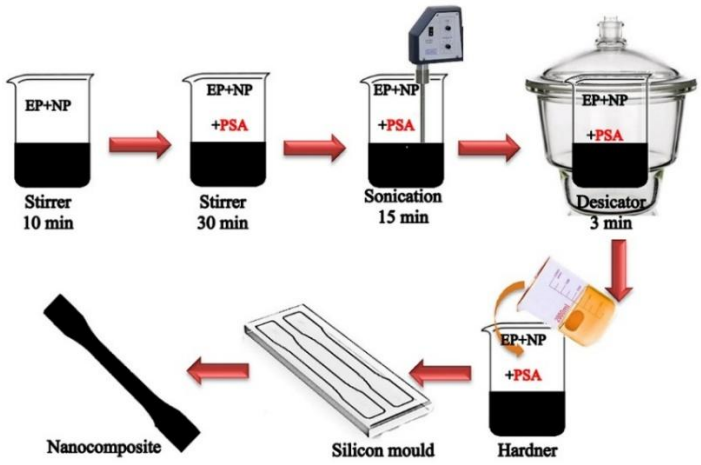

Fig. 1. Schematic representation of the Epoxy/PSA/CF/SiO_2 nanocomposite preparation.

broadening. This method takes into account both the crystallite size and lattice strain as factors contributing to the broadening of the diffraction peaks. The W-H equation is given by:

$$\beta \cos\theta = \frac{K\lambda}{D} + 4\varepsilon \sin\theta \quad (1)$$

where β represents the full width at half

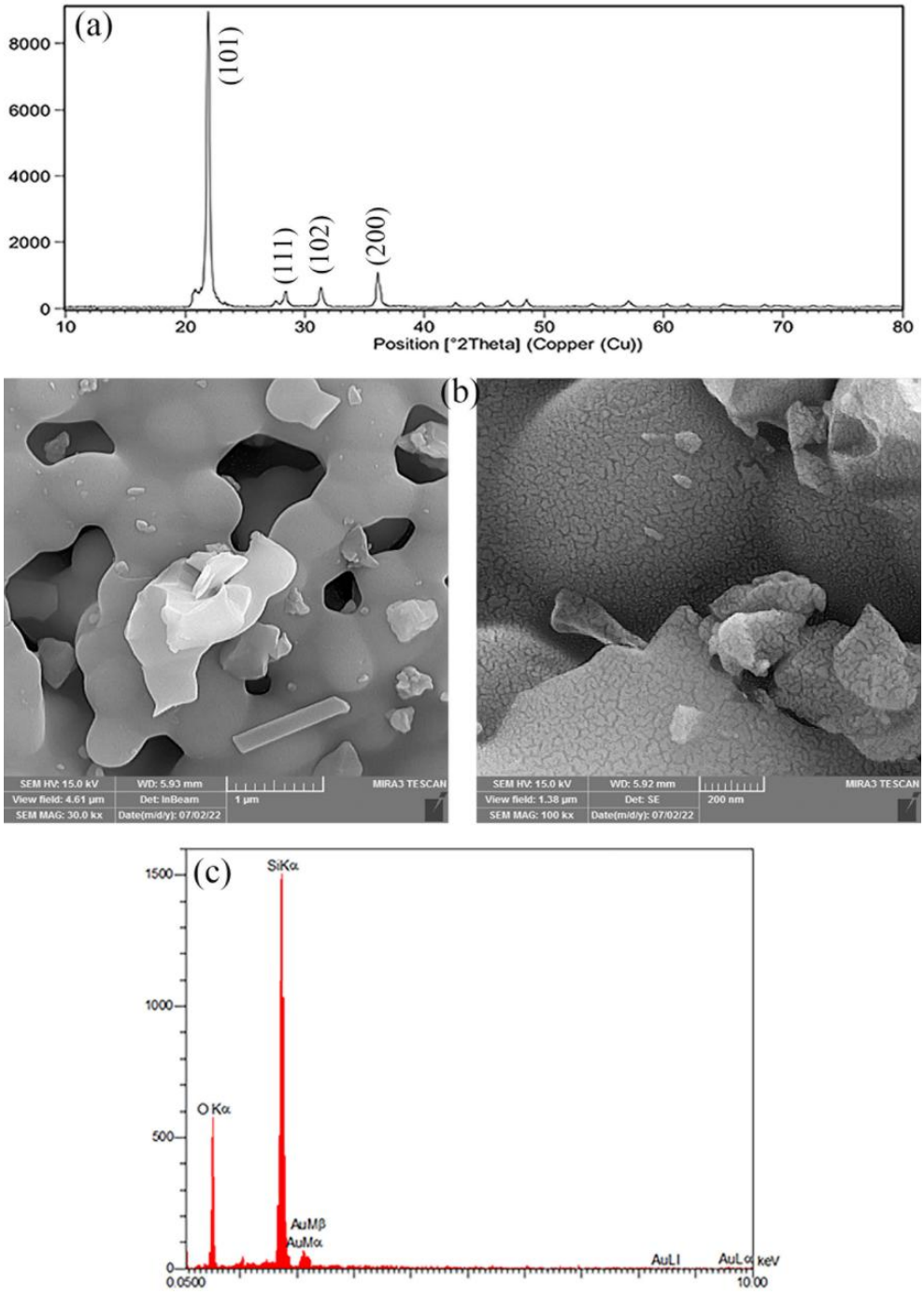

Fig. 2. The XRD pattern (a), the SEM image with various magnifications (b), and EDX images (c) of SiO_2 nanoparticles.

maximum (FWHM) in radians, θ is the Bragg angle, λ is the X-ray wavelength (0.154 nm), K is the shape factor (0.9), and D is the crystallite size. By performing linear regression on the W-H plot, a slope of approximately 0.0021 was obtained, indicating a microstrain of ε ≈ 0.0021 (or 0.21%). This suggests that the SiO_2 nanoparticles synthesized possess a relatively low microstrain and minimal lattice distortions. Furthermore, the intercept of the W-H plot was approximately 0.0037, which corresponds to an average crystallite size of D ≈ 37 nm. These results demonstrate that the synthesized SiO_2 nanoparticles have a uniform size distribution, high crystallinity, and minimal lattice strain.

In Fig. 2(b), SEM images of the surface morphology of silica particles at various magnifications are shown. The sample's morphology primarily consists of micro flakes and irregular rod shapes with agglomeration. The presence of Si and O in the EDAX spectrum confirms the purity of the SiO_2 nanopart icles (Fig. 2(c)).

Response Surface Methodology of Epoxy/PSA/CF/SiO_2 Nanocomposites

The results of the tensile test and the corresponding stress vs. strain curves for the Epoxy/PSA/CF/SiO_2 nanocomposite samples are presented in Table 2.*Analysis of Variance (ANOVA)*

Table 3. ANOVA for Stress (N/m^2) of Epoxy/PSA/CF/SiO_2 nanocomposite.

Source	Sum of Squares	df	Mean Square	F-value	p-value	
Model	1589.77	9	176.64	5.02	0.0094	significant
A-NP	44.78	1	44.78	1.27	0.2855	
B-Fiber	1329.71	1	1329.71	37.82	0.0001	
C-PSA	7.49	1	7.49	0.2129	0.6544	
AB	19	1	19	0.5405	0.4791	
AC	17.97	1	17.97	0.5111	0.491	
BC	115.75	1	115.75	3.29	0.0997	
A^2	4.38	1	4.38	0.1247	0.7314	
B^2	36.56	1	36.56	1.04	0.3319	
C^2	13.48	1	13.48	0.3832	0.5497	
Residual	351.62	10	35.16			
Lack of Fit	284.07	5	56.81	4.2	0.0705	not significant
Pure Error	67.56	5	13.51			
Cor Total	1941.39	19				
Std. Dev.	5.93		R^2	0.8189	Mean	49.5
Adjusted R^2	0.6559		C.V. %	11.98	Predicted R^2	-0.1627
			Adeq Precision	9.1472		

Table 4. ANOVA for Strain (N/m^2) of Epoxy/PSA/CF/SiO_2 nanocomposite.

Source	Sum of Squares	df	Mean Square	F-value	p-value	
Model	18.69	9	2.08	4.05	0.0199	significant
A-NP	1.21	1	1.21	2.35	0.1559	
B-Fiber	3.1	1	3.1	6.05	0.0337	
C-PSA	0.8514	1	0.8514	1.66	0.2266	
AB	1.1	1	1.1	2.14	0.1746	
AC	0.405	1	0.405	0.7898	0.395	
BC	0.8844	1	0.8844	1.72	0.2184	
A^2	5.52	1	5.52	10.77	0.0083	
B^2	0.4075	1	0.4075	0.7946	0.3936	
C^2	4.19	1	4.19	8.16	0.017	
Residual	5.13	10	0.5128			
Lack of Fit	3.45	5	0.6897	2.05	0.2242	not significant
Pure Error	1.68	5	0.3358			
Cor Total	23.82	19				
Std. Dev.	0.7161		R^2	0.7847	Mean	8.93
Adjusted R^2	0.591		C.V. %	8.02	Predicted R^2	-0.2249
			Adeq Precision	8.2848		

The results of the analysis of variance (ANOVA) for stress, strain, and area are presented in Tables 3 to 5. These tables indicate that these parameters have a significant impact on the responses and that the models fit the experiment well, as the lack of fit is not significant. P values below 0.05 indicate that the parameters have a significant effect on the responses. Furthermore, the regression coefficients (R^2) for stress, strain, area, modulus, and yield are 0.81, 0.78, 0.75, 0.92, and 0.92, respectively, demonstrating a strong correlation between the experimental and anticipated values.

The final equation in terms of the actual factors is as follows:

$$Stress=22-6.04A+40.72B+4.29C-4.35AB+1.69AC-4.3BC+1.55A^2-4.5B^2-0.43C^2 \quad (2)$$

$$Strain=6.11-2.31A+1.83B+2.01C-1.04AB-0.25AC-0.37BC+1.75A^2+0.47B^2-0.24C^2 \quad (3)$$

$$Area=108.48-108.02A+549.44B+193.28C-101.87AB+21.79AC-84.54BC+62.62A^2+9.44B^2-25.91C^2 \quad (4)$$

$$Modulus=6.54-1.47A+6.59B-1.01C+0.32AB+0.29AC-0.34BC+.0049A^2-1.78B^2+0.16C^2 \quad (5)$$

$$Yield=19.16-5.93A+42.93B+4.46C-4.22AB+1.57AC-4.26BC+1.64A^2-5.56B^2-0.44C^2 \quad (6)$$

The optimum percentage weight of PSA, CF, and SiO_2 NPs for fabricating nanocomposites with maximum mechanical properties, along with the obtained experimental values, is shown in Table 6.

Plots of Predicted versus Actual Values

Fig. 3 shows the comparison of predicted and actual values for stress, strain, area, modulus, and yield. The graph indicates a strong agreement between the predicted and actual values, as the points closely align with each other. This demonstrates a high level of agreement between the two sets of values.

2D and 3D Response surface plots

The contour and response surface plots of the Epoxy/PSA/CF/SiO_2 nanocomposite, generated from the empirically predicted model as shown in Figs. 4 to 6, can be used to better assess the overall relationship between the independent variables (fiber, nanoparticle (NP), and polystyrene acrylic

Table 5. ANOVA for Area (J/m^3) of Epoxy/PSA/CF/SiO_2 nanocomposite.

Source	Sum of Squares	df	Mean Square	F-value	p-value	
Model	4.358E+05	9	48420.34	3.37	0.0359	significant
A-NP	4387.87	1	4387.87	0.3056	0.5925	
B-Fiber	3.142E+05	1	3.142E+05	21.88	0.0009	
C-PSA	28.47	1	28.47	0.0020	0.9654	
AB	10378.08	1	10378.08	0.7229	0.4151	
AC	2969.89	1	2969.89	0.2069	0.6590	
BC	44673.59	1	44673.59	3.11	0.1082	
A^2	7065.68	1	7065.68	0.4921	0.4990	
B^2	160.64	1	160.64	0.0112	0.9178	
C^2	47250.98	1	47250.98	3.29	0.0997	
Residual	1.436E+05	10	14357.05			
Lack of Fit	1.103E+05	5	22068.63	3.32	0.1069	not significant
Pure Error	33227.36	5	6645.47			
Cor Total	5.794E+05	19				
Std. Dev.	119.820		R^2	0.7521	Mean	662.788
Adjusted R^2	0.5291		C.V. %	18.078	Predicted R^2	-0.5621
			Adeq Precision	6.2223		

Table 6. The optimum weight percentage of components in the fabrication of Epoxy/PSA/CF/SiO_2 nanocomposites and the results of the validation experiment.

Optimized property	Symbol	optimum percentage weight			Experimental Response		
		PSA	CF	SiO_2 Nps	Stress	Strain	Area
Stress	EPCSN(Stress)	1.11	1.59	0.4	72.76	11.15	1032.35
Strain	EPCSN(Strain)	2.69	1.59	0.4	59.60	12.30	940.15
Area	EPCSN(Area)	1.29	1.59	0.4	67.39	9.74	1035.09

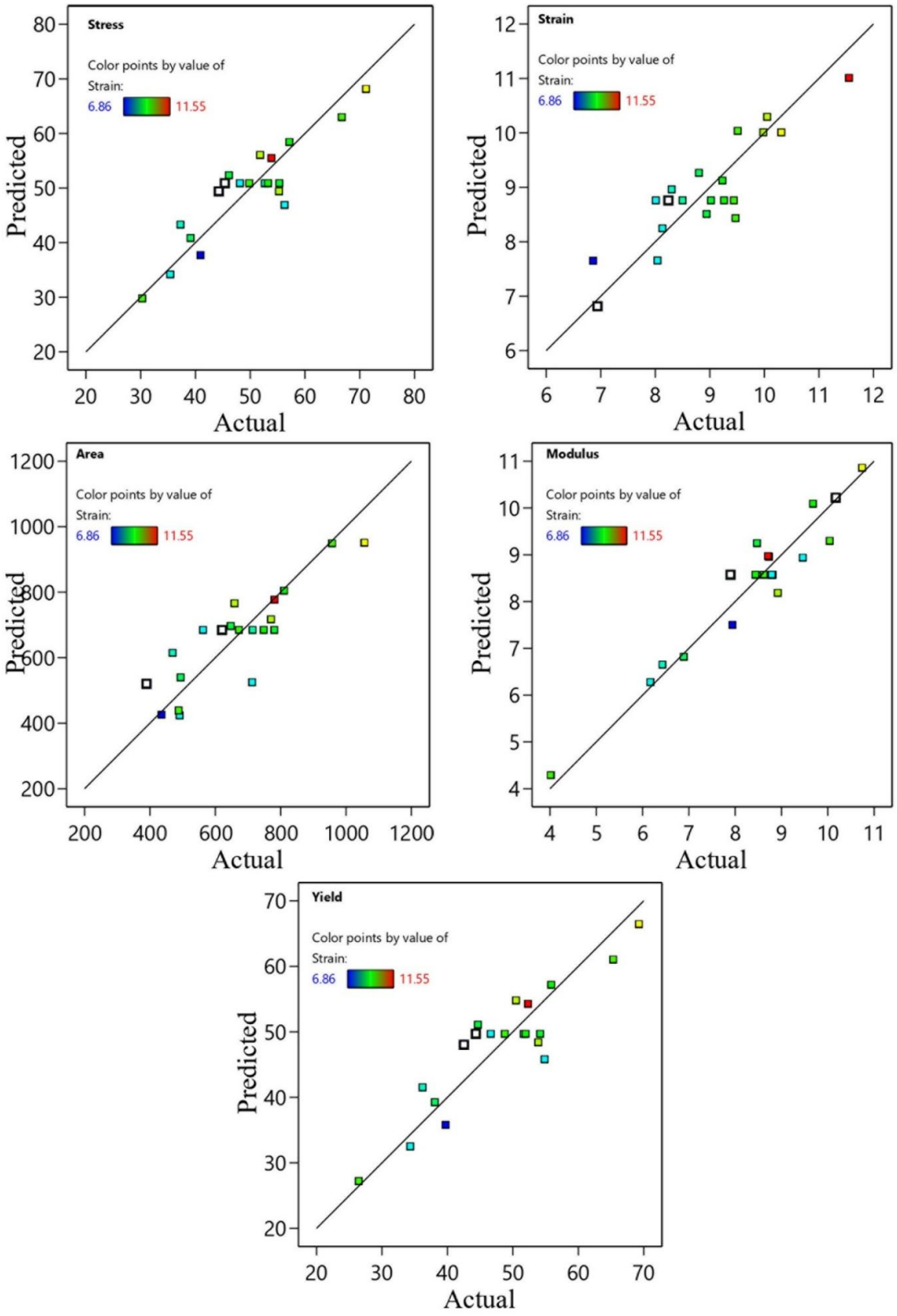

Fig. 3. Plots of predicted versus actual values for stress, strain, area, modulus, and yield of Epoxy/PSA/CF/SiO_2 nanocomposite.

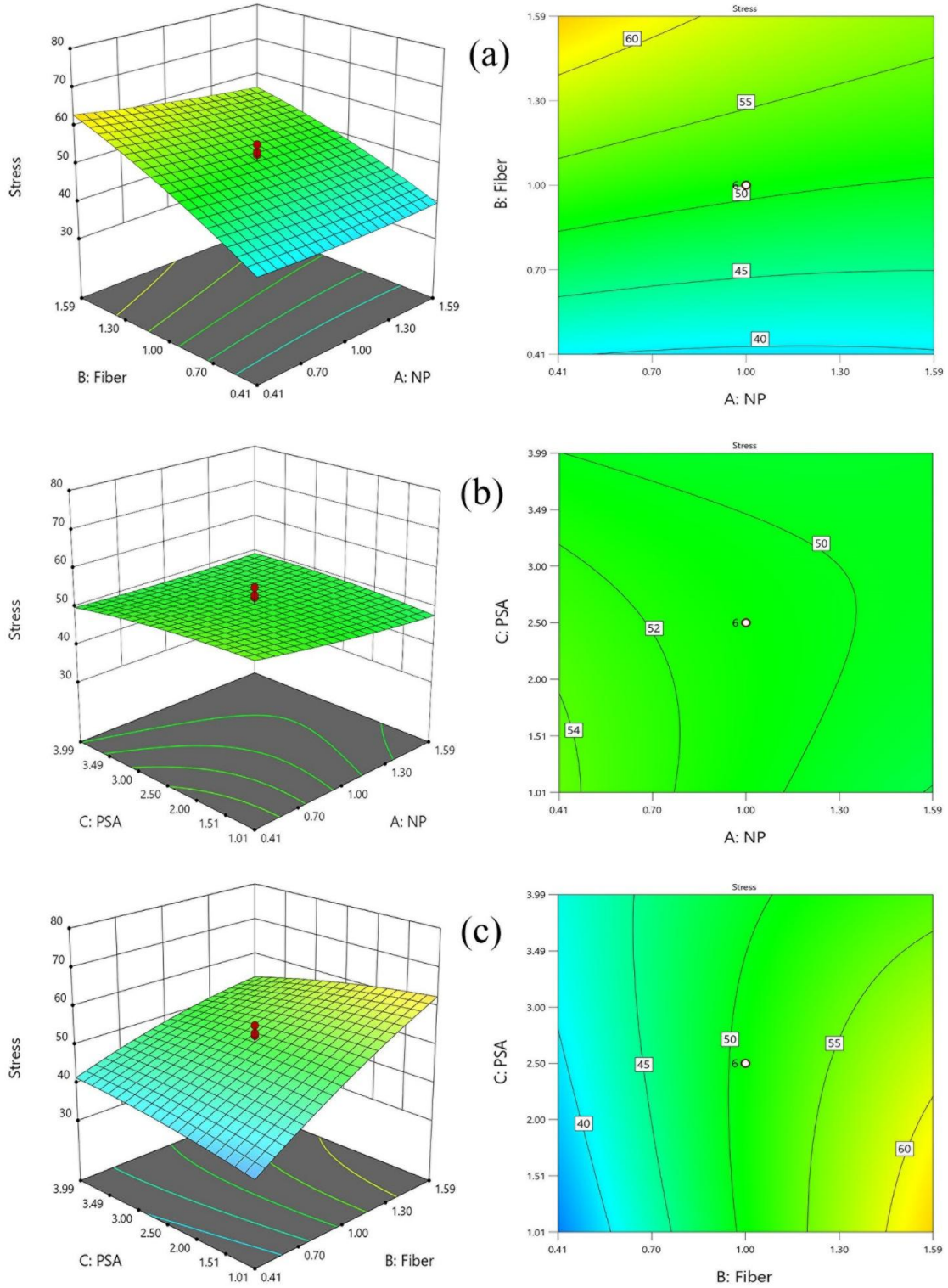

Fig. 4. 3D surface (left) and 2D contour plots (right) for the effect of PSA, CF, and SiO_2 NPs percentages on the stress parameter of Epoxy/PSA/CF/SiO_2 nanocomposite.

(PSA)) and the response variables (stress, strain, area, modulus, and yield). The two-dimensional (2D) contour plot, which is depicted by holding the other variables at their center point level, demonstrates the mutual interaction of the independent factors.

Stress

As shown in Fig. 4, several response surface plots are developed to determine the optimum condition of each variable toward the maximum stress by converting the mutual interaction between two targeted variables on stress into a three-dimensional (3D) diagram. Figs. (4(a) and 4(c)), presenting the mutual interaction of the fiber percentage with nanoparticles and polystyrene acrylic, respectively, confirm the higher intensity of the effect of the fiber percentage on stress compared with these factors. An increase in carbon fiber from 0.4 wt% to 1.59 wt% led to an improvement in stress. Also, the stress, which is brought on by the agglomeration of nanoparticles, is marginally reduced by the increase of SiO_2 NPs from 0.4 %wt to 1.59 %wt.

Nanoparticles strive to achieve a stable size of a few microns by forming powerful agglomerates through the use of van der Waals forces. This is necessary because their small size and large specific surface area make them highly unstable [18]. In Fig. 4(b), it can be observed that there was a slight increase in stress as the amounts of nanoparticles and PSA decreased. However, according to Table 4, only the primary variable B (carbon fiber) showed significance, while variables A (NP) and C (PSA) did not, as their p-values were higher than 0.05. It is worth noting that the larger the F-value, the stronger the effect of the variables [19]. The F-values indicate that the fiber content (variable B) with F = 37.82 units has a significantly higher impact on stress compared to the SiO_2 NPs (F = 1.27 units) and PSA (F = 0.2129) variables. This suggests that the fiber content has the strongest influence on stress, while the amount of SiO_2 nanoparticles and PSA has a relatively minimal impact. The primary variables can be ranked in the following order: C, A, and B, respectively.

Strain

To further analyze and investigate the interaction between strain and variables (SiO_2 Nps, PSA, and Carbon fiber), Fig.s 5 show the graphical response surface plot (3D) and contour plot (2D). When the interaction effect between these parameters is insignificant, the response surface for a polynomial model will be a flat plane. However, if the interaction effect is significant, the plane will curve or bend. This indicates that the underlying regression model for the experiment has a curvature due to the interaction effect [20]. The twisted response surface curves indicate a significant interaction between variables.

Fig. 5(a) illustrates that the strain of Epoxy/PSA/CF/SiO_2 nanocomposites increases with the addition of carbon fiber. As the amount of nanoparticles increases, the strain initially decreases and then increases again. The strain reaches its peak at a high level of carbon fibers and a low level of nanoparticles. In addition, the use of nanoparticles in nanocomposites improves the strength of the interface and significantly alters stress and strain propagation [21]. Figs. 5(a) and 5(b) demonstrate that with an NP concentration of 0.40 wt%, an increase in PSA to 3 wt% results in a gradual increase in strain.

Area

Fig. 6 displays the interaction effects of the process parameters on area in 3D surface and 2D contour plots. These graphs demonstrate the simultaneous effects of two factors while maintaining the central value of another parameter. Figs. 6(a) illustrates that the area increases as the percentage of SiO_2 nanoparticles increases at the highest weight percentage of carbon fiber. Figs. 6(b) shows that at the low level of SiO_2 nanoparticles, the addition of 1 wt% PSA increases the area to the highest level. Figs. 6(c) demonstrates that, at the maximum weight percentage of carbon fiber, the area increases as the weight percentage of PSA decreases.

Characterization of Epoxy/PSA/CF/SiO_2 nanocomposites

Fourier transform infrared (FTIR) spectroscopy analysis

The FT-IR spectra of the Epoxy, Epoxy/2.69%PSA composite (Epoxy/PSA), EPCSN(Area), EPCSN(Strain), and EPCSN(Stress) nanocomposites are shown in Fig. 7. After adding a small amount of SiO_2 NPs, PSA, and carbon fiber to the Epoxy, all of the spectra display similar vibrational patterns in the spectral region, indicating that there have been no significant changes to the chemical bonds and structures in the epoxy resins.

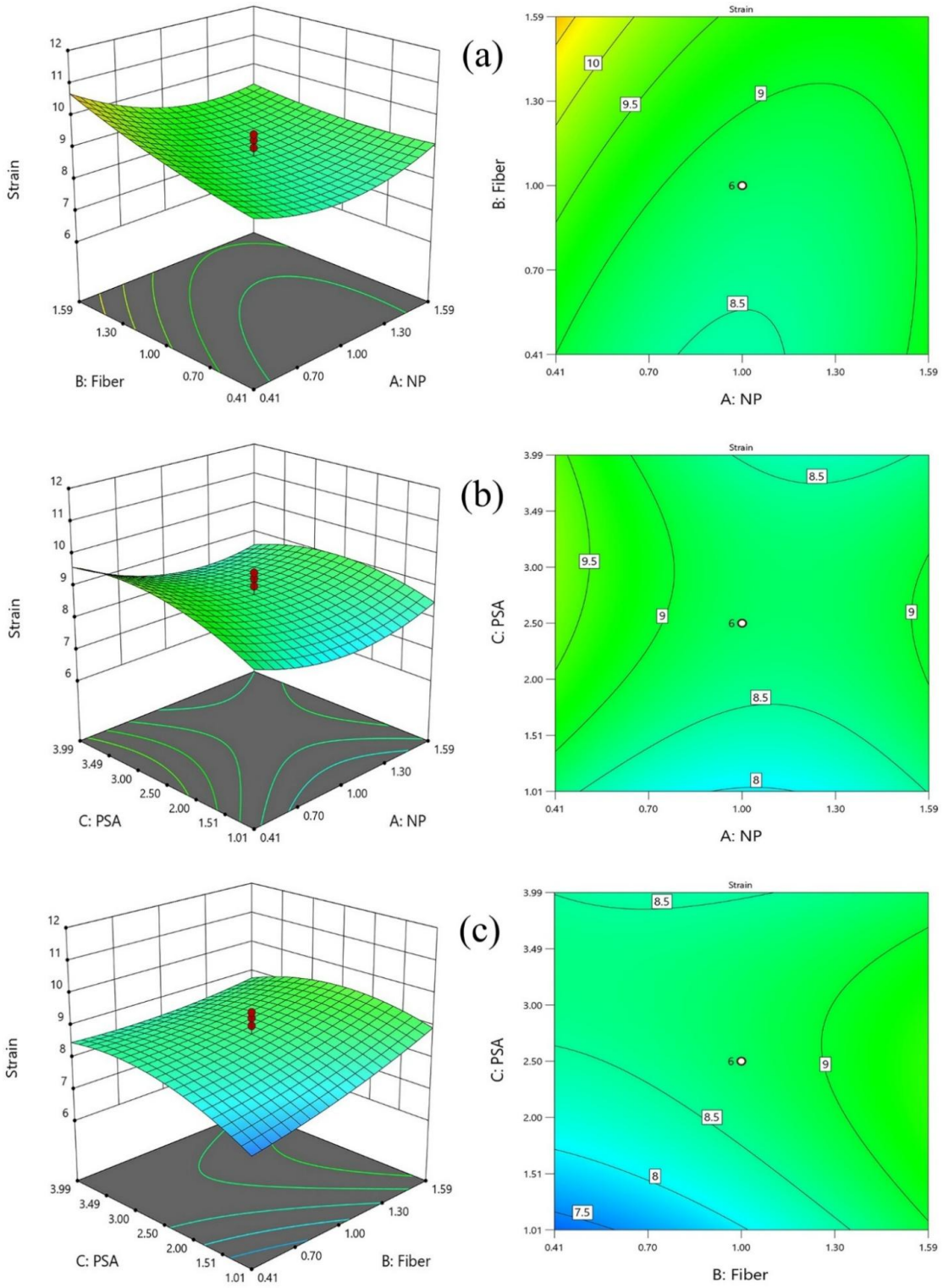

Fig. 5. 3D surface (left) and 2D contour plots (right) for the effect of PSA, CF, and SiO_2 NPs percentages on the strain parameter of Epoxy/PSA/CF/SiO_2 nanocomposite.

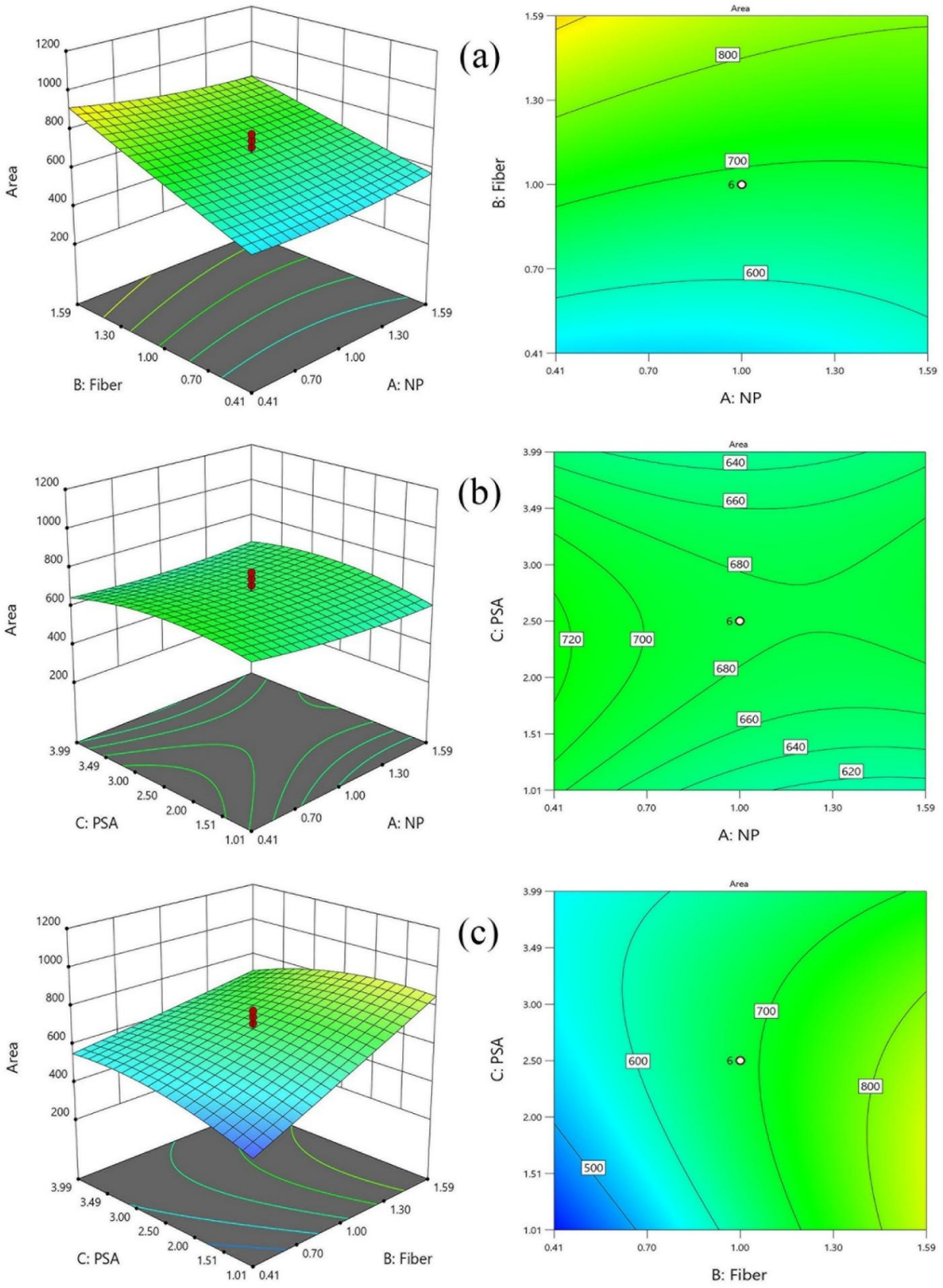

Fig. 6. 3D surface (left) and 2D contour plots (right) for the effect of PSA, CF, and SiO_2 NPs percentages on the Area parameter of Epoxy/PSA/CF/SiO_2 nanocomposite.

The FTIR spectra of the nanocomposites show peaks from the aromatic core of the diglycidyl ether of bisphenol-A (830, 1030, 1180, 1225, 1510, and 1610 cm^{-1}) and the aliphatic ether linkage (1035 cm^{-1}) [22-24]. The disappearance of the characteristic peak at 915 cm^{-1}, which corresponds to the oxirane group of DGEBA, indicates that the epoxy resin is fully cured [22].

Another prominent signal is the broad peak at 3400 cm^{-1}, which corresponds to the stretching of OH bonds [25]. Additionally, the band observed at 2925 cm^{-1} is attributed to the vibration of aromatic protons [26].

X-ray diffraction (XRD) analysis

Fig. 8 shows the X-ray diffraction (XRD) pattern of pure epoxy resin and its composites. The XRD analysis provides valuable information on the structural properties of the composites and is crucial in detecting the dispersion of NPs and the

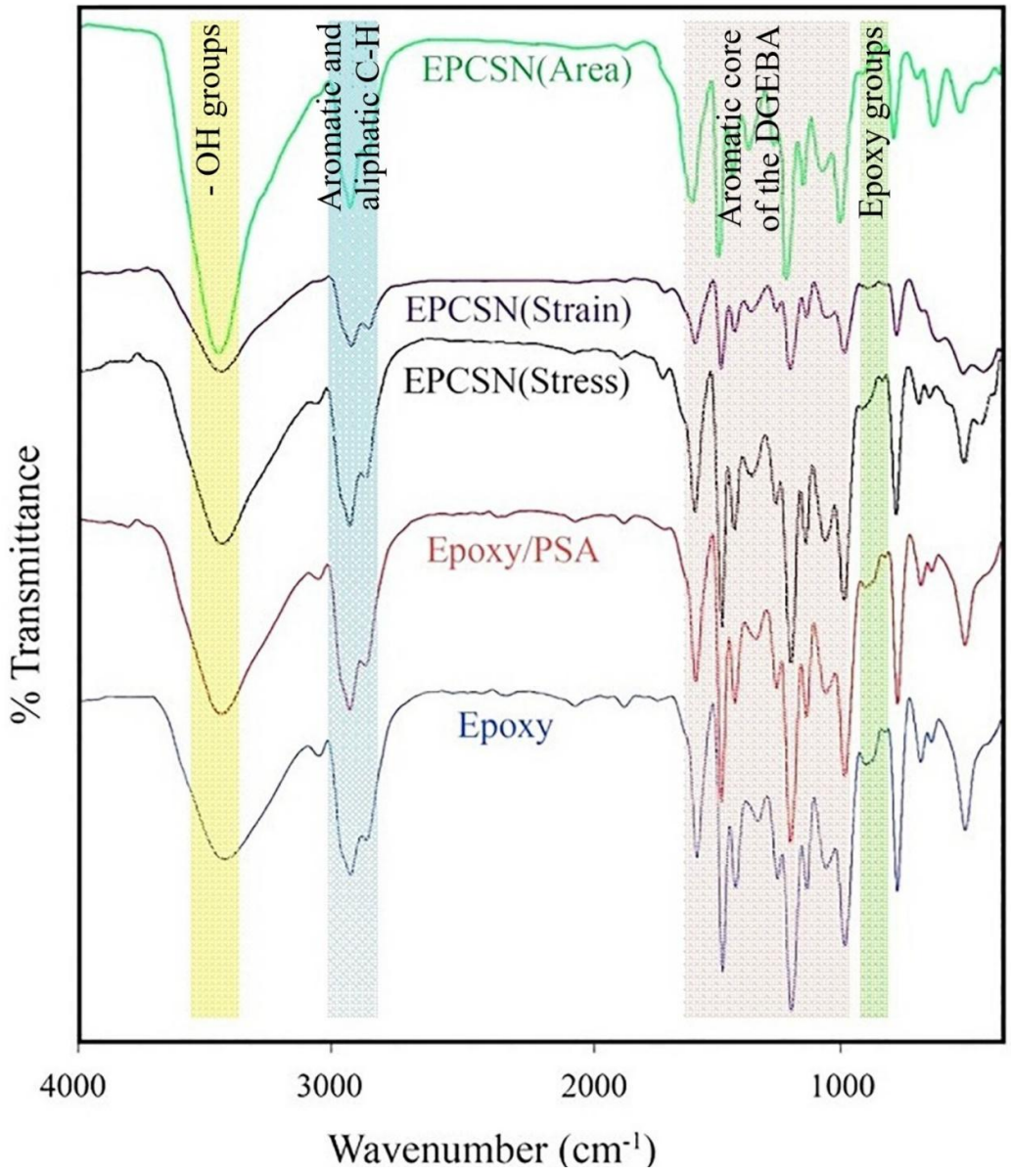

Fig. 7. The FT-IR spectra of the Epoxy, Epoxy/PSA, and EPCSN nanocomposites.

extent of their exfoliation and intercalation within the epoxy resin matrix [27]. The pure epoxy resins exhibit wide peaks in their diffraction patterns. These patterns typically display broad diffraction from 5-80°, with a few distinct peaks occurring between 20-45°. This scattering of the cured epoxy network allows for the revelation of its amorphous nature [27, 28]. The XRD pattern of the epoxy nanocomposites are revealed weak intensities for the epoxy diffraction peaks after the dispersion of SiO_2 in the epoxy matrix.

The crystalline phase area was measured as 8983.1334, while the amorphous phase area was 5390.7070. Using Equation 1, the crystallinity percentage was calculated to be approximately 62.5%, indicating a significant crystalline content with a notable amorphous fraction. This is consistent with the synthesis conditions and structural characteristics of the low-cristobalite phase.

$$\text{Crystallinity percentage} = \frac{\text{Area of Crystalline Peaks}}{\text{Total Area}} \times 100 \quad (7)$$

The crystallinity percentage of the epoxy nanocomposites was determined by analyzing their XRD patterns. The results show that the samples Epoxy+1.11%PSA, EPCSN (Strain), EPCSN (Area), and pure epoxy have crystallinity percentages of 2.46%, 4.8%, 4.1%, and 16.9%, respectively. The variations in crystallinity among these samples can be attributed to differences in the dispersion of nanoparticles and their interactions with the epoxy matrix. Scientific studies have shown that factors such as the concentration and type of additives can affect the degree of crystallinity by altering the packing of polymer chains and creating amorphous regions. This can lead to a decrease in crystallinity, especially with higher levels of nanofillers due to increased interfacial interactions.

After incorporating SiO_2 nanoparticles into the epoxy matrix, the intensity of the X-ray diffraction (XRD) peaks decreased significantly from ≈2000 to ≈500. This decrease in peak intensity is typically indicative of a decrease in crystalline order or an increase in the amorphous fraction of the sample. Since SiO_2 nanoparticles are known to have a semi-amorphous/amorphous nature, their homogeneous dispersion within the polymer

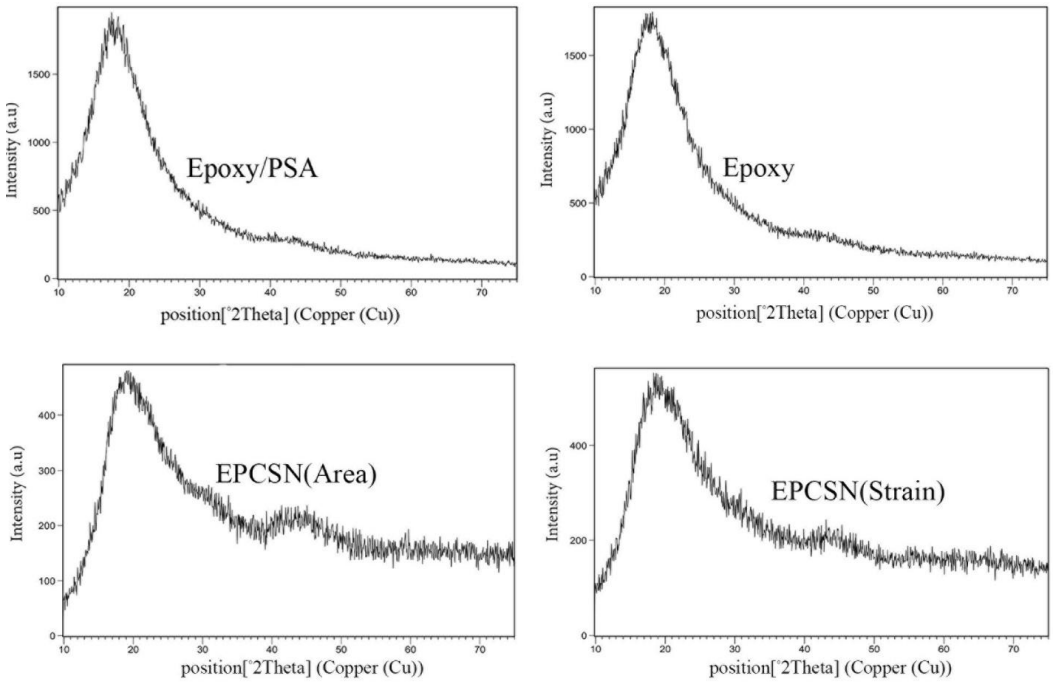

Fig. 8. XRD pattern for (a) Epoxy, (b) Epoxy/PSA, (c) EPCSN(Stress), and (d) EPCSN(Strain).

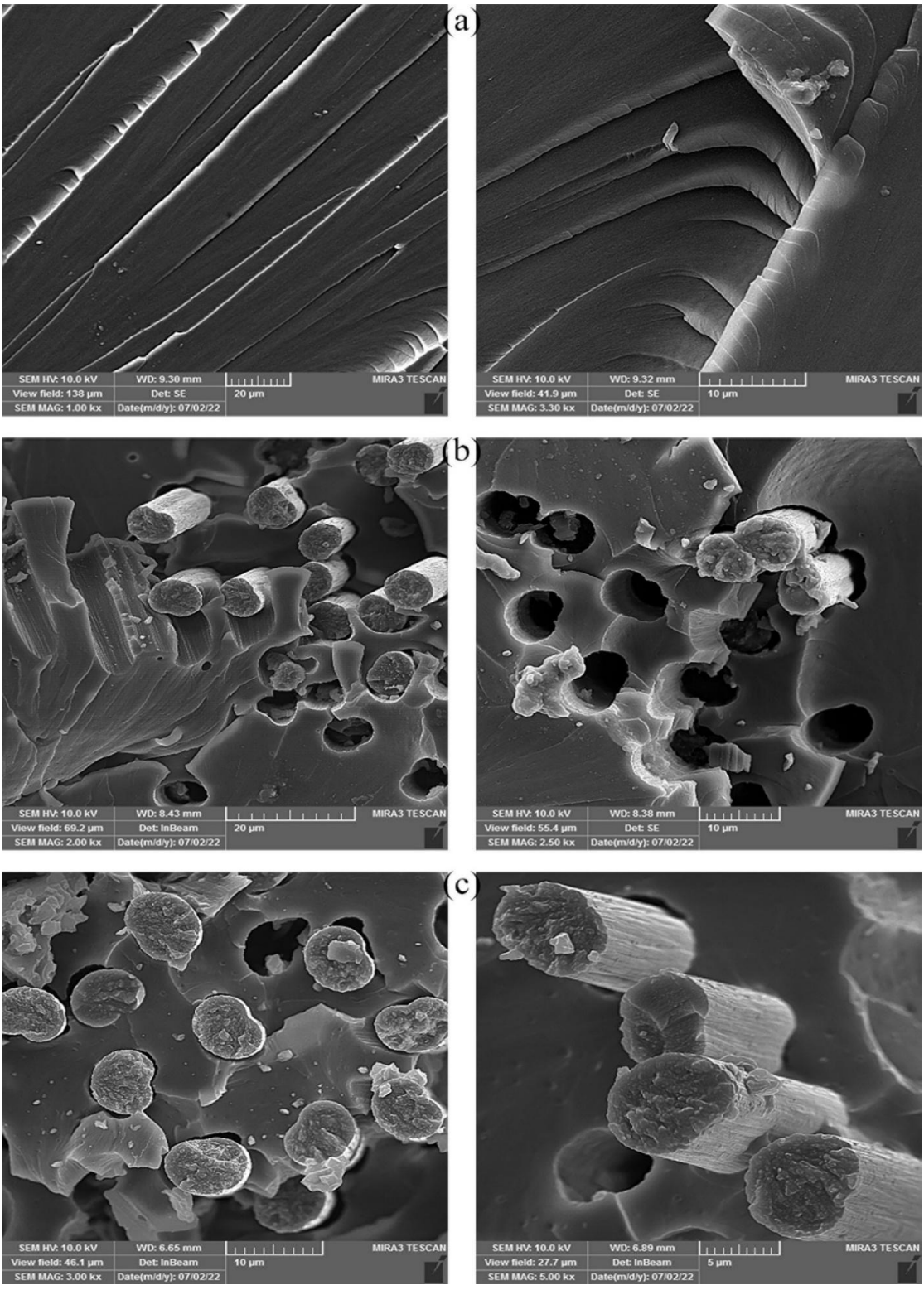

Fig. 9. Cross section SEM images of (a) Epoxy/PSA, (b) EPCSN(Area), and (c) EPCSN(Strain).

matrix can lead to broadening and attenuation of the characteristic peaks of the host material. Additionally, the process of exfoliation or the distribution of the particles at the nanoscale level may contribute to local structural disorder, resulting in a reduction in the sharpness and intensity of the diffraction peaks. This behavior is consistent with previous studies, which have shown the appearance of broad and weak peaks around $2\theta \approx 23°$ for samples containing SiO_2. These findings are further supported by TEM imaging and calculations of the crystallinity index, which confirm the amorphous nature of the incorporated SiO_2 phase.

The maximum intensity of the cured epoxy resin decreased at a concentration of 0.4 wt.% of SiO_2 nanoparticles. Furthermore, the position of the broad hump peak in the XRD pattern of the Epoxy/PSA/CF/SiO_2 nanocomposite remained unchanged, while the intensity of the broad hump in the pristine epoxy continued to decrease. This suggests that the addition of SiO_2 nanoparticles to the epoxy matrix did not affect the structure or formation of new phases [24, 28].

Scanning electron microscope (SEM) and Energy-dispersive X-ray spectroscopy (EDX)

The cross-sectional SEM images, along with EDX analysis, of the Epoxy/PSA composite and Epoxy/PSA/CF/SiO_2 nanocomposite at various magnifications are shown in Fig. 9 and Fig. 10, respectively. While the Epoxy/PSA/CF/SiO_2 nanocomposites exhibit a heterogeneous morphology, the cross-sectional SEM of the Epoxy/PSA composite displays a smooth and homogeneous microstructure. The surface micrograph of these nanocomposites reveals the presence of carbon fibers and silica nanoparticles. The SEM images clearly show the dispersion of silica nanoparticles in nanocomposites. Additionally, the fracture surface appears to be varied and contains holes. The chemical textures of the Epoxy/PSA composite and Epoxy/PSA/CF/SiO_2 nanocomposite surfaces also exhibit noticeable differences. As seen in Fig. 10, the EDX analysis confirms the purity of these samples and

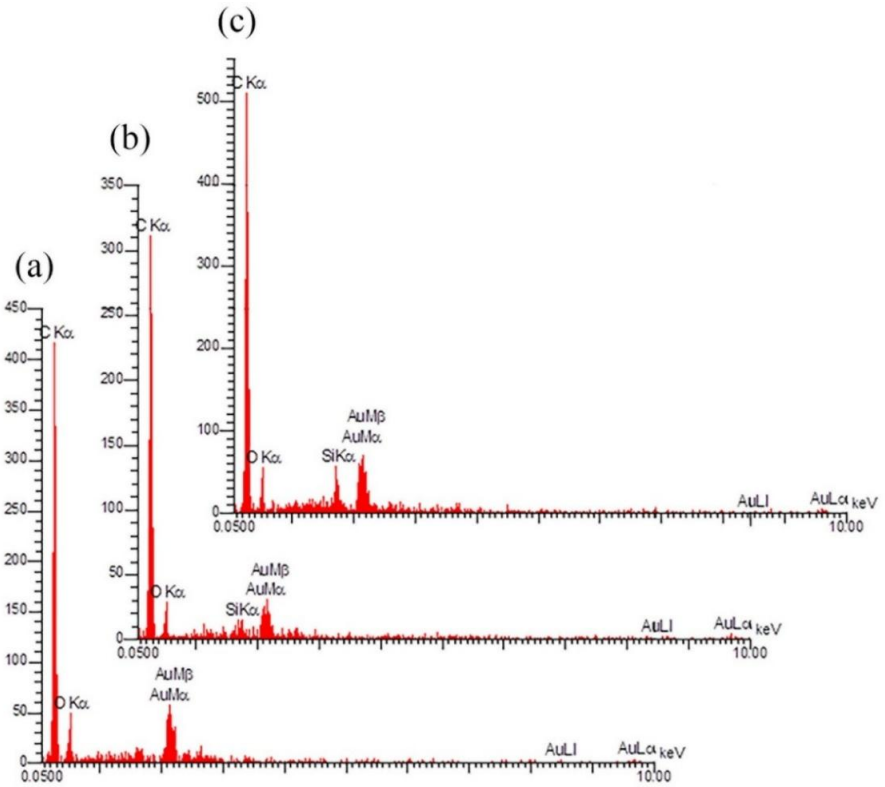

Fig. 10. The EDX analysis of (a) Epoxy/PSA, (b) EPCSN(Area), and (c) EPCSN(Strain).

reveals the presence of elements such as carbon, oxygen, and silicon.

Thermogravimetric analysis (TGA)

Thermogravimetric (TGA) analysis was conducted on three samples: Epoxy/PSA composite, EPCSN(Area), and EPCSN(Strain) nanocomposite are presented in Fig. 11. The purpose of this examination was to investigate the effect of adding SiO_2 and PSA on the thermal behavior of the composites. The initial weight loss occurred at temperatures ranging from 70 to 300 °C, with the EPCSN(Strain) nanocomposite showing the highest loss due to moisture absorption [29]. The degradation of the polymer chain is linked to the second stage, which occurs at approximately 300 °C. According to the results, the nanocomposite with 1.29% PSA exhibited greater thermal stability than the nanocomposite with 2.69% PSA. The data indicate that the composites/nanocomposites experience a higher weight loss in the presence of PSA compared to other samples. In conclusion, Fig. 12 demonstrates the impact of the interactions between carbon fiber,

Table 7. Comparison of Mechanical Properties of the Present Study with Developed Nanocomposites and Commonly Used Fillers in the Literature.

Filler	Mechanical properties				Ref.
	Elongation	Modulus	Stress	Toughness	
53.5 vol% CF	72.2% ↓	1927% ↑	1045% ↑		[30]
30 vol% CF		2761% ↑	809% ↑		[31]
3 wt% SiO_2			18.45% ↑	120% ↑	[32]
2 wt% SiO_2		58.9% ↑			[33]
0.89 wt% CF + 1 wt% SiO_2				33% ↑	[34]
60 wt % CF + 1.5 wt% SiO_2		11.2% ↑	8.2% ↑		[35]
EPCSN(Stress)	46.5% ↓	163.3 ↑	88.54% ↑	38.4% ↓	present study
EPCSN(Strain)	41.0% ↓	103.3% ↑	54.4 % ↑	43.9% ↓	present study

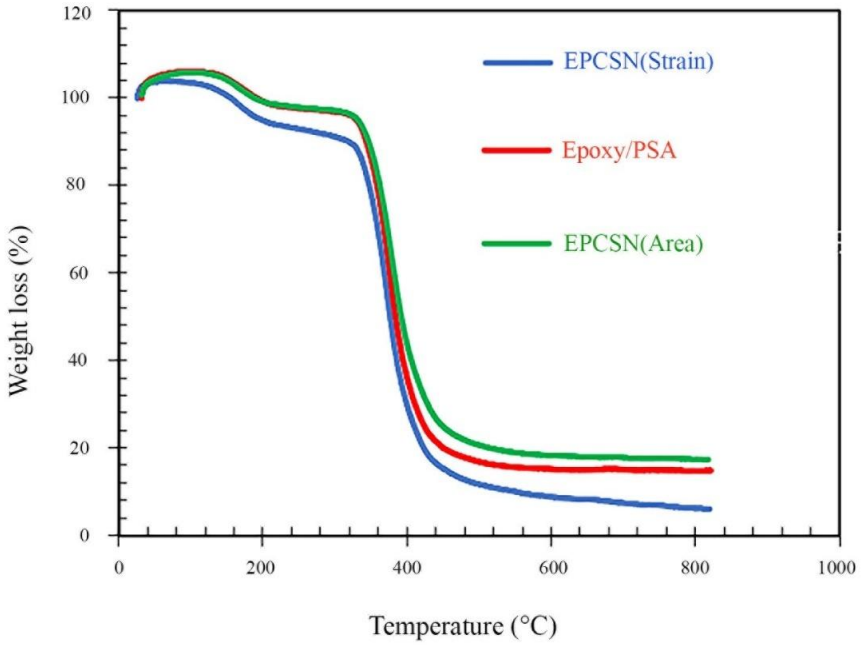

Fig. 11. TGA curves of (a) Epoxy/PSA, (b) EPCSN(Area), and (c) EPCSN(Strain).

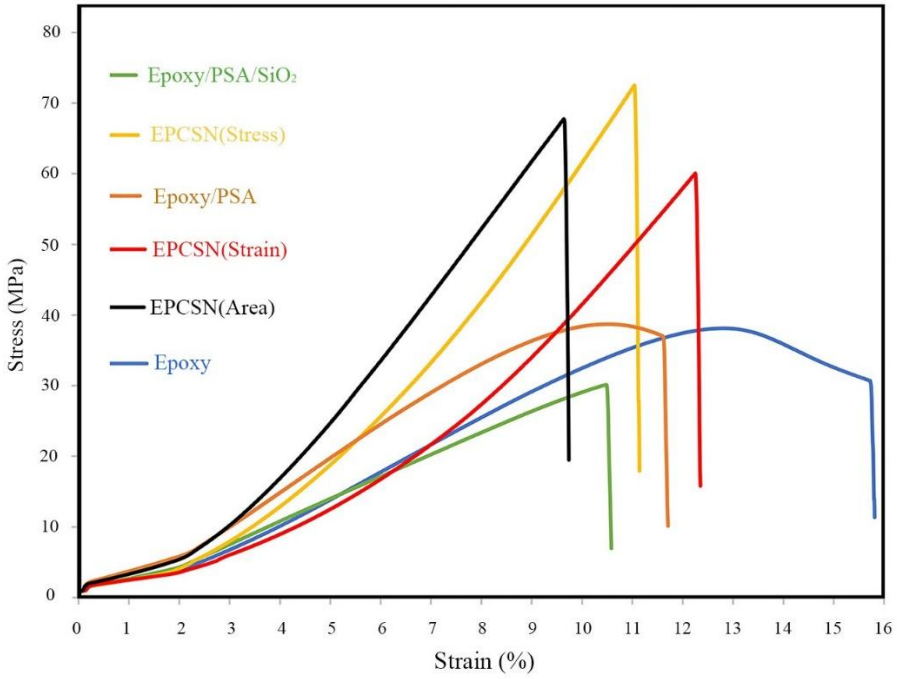

Fig. 12. Strain-vs-strain curves for Epoxy, Epoxy/PSA composite, Epoxy/PSA/SiO2 and optimized nanocomposites.

nanofiller, and PSA on the tensile properties of the nanocomposite.

CONCLUSION

The objective of this study is to enhance the properties of carbon fiber-reinforced composites through the incorporation of polystyrene, acrylic, and SiO_2 nanoparticle fillers. The inclusion of SiO_2 Nps and polystyrene acrylic resulted in significant improvements in the stress, strain, and area of the composite. Specifically, the addition of 0.41 wt% SiO_2 Nps filler and 1.59 wt% carbon fiber to epoxy resin led to a substantial increase in stress, strain, and area. The stress for pure epoxy is 38.59 MPa. However, when combined with 1.11% wt PSA, 1.59% wt CF, and 0.41% wt SiO_2, the resulting nanocomposites exhibit a significantly higher stress of 72.76 MPa, representing an impressive 88.54% improvement. The pure epoxy strain is 15.83%, while the maximum strain of 12.3% is observed in the EPCSN(Strain) nanocomposites, resulting in a 22.3% decrease in strain. The area for pure epoxy is 1152.78 j, while the area of the EPCSN(Area) nanocomposites is 1035.09, resulting in a reduction of 10.21 j in area. The results of the tensile test for the Epoxy/PSA/CF/SiO_2 nanocomposites showed a correlation between the weight percentages of SiO_2, carbon fiber, and PSA. However, it was observed that the presence of high concentrations of SiO_2 led to a decrease in the area, stress, and strain of the nanocomposite. This could be attributed to the agglomeration of SiO_2 and propagation of fractures, resulting in reduced tensile strength. The mechanical properties of the nanocomposite developed in this study, as reported in Commonly Used Fillers in the Literature, are compared in Table 7. The results in this table indicate that a significant rise in carbon fiber content leads to a decrease in the elongation and toughness of the nanocomposite, despite an accompanying increase in stress. The use of PSA and SiO_2 nanoparticles in the nanocomposite effectively balances the effects of the carbon fiber.

ACKNOWLEDGMENTS

The authors are grateful to the university of Kashan for supporting this work by Grant No.

1222034.

CONFLICT OF INTEREST

The authors declare that there is no conflict of interests regarding the publication of this manuscript.

REFERENCES

1. Goyat MS, Hooda A, Gupta TK, Kumar K, Halder S, Ghosh PK, et al. Role of non-functionalized oxide nanoparticles on mechanical properties and toughening mechanisms of epoxy nanocomposites. Ceram Int. 2021;47(16):22316-22344.
2. Sheth D, Maiti S, Patel S, Kandasamy J, Chandan MR, Rahaman A. Enhancement of mechanical properties of carbon fiber reinforced epoxy matrix laminated composites with multiwalled carbon nanotubes. Fullerenes, Nanotubes and Carbon Nanostructures. 2020;29(4):288-294.
3. Jain V, Bisht A, Jaiswal S, Dasgupta K, Lahiri D. Assessment of Interfacial Interaction in Graphene Nanoplatelets and Carbon Fiber-Reinforced Epoxy Matrix Multiscale Composites and Its Effect on Mechanical Behavior. J Mater Eng Perform. 2021;30(12):8913-8925.
4. Mirsalehi SA, Youzbashi AA, Sazgar A. Enhancement of out-of-plane mechanical properties of carbon fiber reinforced epoxy resin composite by incorporating the multi-walled carbon nanotubes. SN Applied Sciences. 2021;3(6).
5. Clifton S, Thimmappa BHS, Selvam R, Shivamurthy B. Polymer nanocomposites for high-velocity impact applications-A review. Composites Communications. 2020;17:72-86.
6. Cao X, Li J. Enhanced interfacial property of carbon fiber reinforced epoxy composite based on carbon fiber treated by supercritical water/nitrate system. J Compos Mater. 2021;55(25):3719-3727.
7. Ma C, Liu H-Y, Du X, Mach L, Xu F, Mai Y-W. Fracture resistance, thermal and electrical properties of epoxy composites containing aligned carbon nanotubes by low magnetic field. Composites Science and Technology. 2015;114:126-135.
8. Sprenger S. Epoxy resin composites with surface-modified silicon dioxide nanoparticles: A review. J Appl Polym Sci. 2013;130(3):1421-1428.
9. Burkov MV, Eremin AV. Mechanical properties of carbon-fiber-reinforced epoxy composites modified by carbon micro- and nanofillers. Polym Compos. 2021;42(9):4265-4276.
10. Ng CB, Ash BJ, Schadler LS, Siegel RW. A Study of the Mechanical and Permeability Properties of Nano- and Micron-TiO_2 Filled Epoxy Composites. Advanced Composites Letters. 2001;10(3).
11. Shanthi M, Gupta M, Jarfors AEW, Tan MJ. Synthesis, characterization and mechanical properties of nano alumina particulate reinforced magnesium based bulk metallic glass composites. Materials Science and Engineering: A. 2011;528(18):6045-6050.
12. Cho J, Chen JY, Daniel IM. Mechanical enhancement of carbon fiber/epoxy composites by graphite nanoplatelet reinforcement. Scripta Mater. 2007;56(8):685-688.
13. He H, Li K, Wang J, Sun G, Li Y, Wang J. Study on thermal and mechanical properties of nano-calcium carbonate/epoxy composites. Materials and Design. 2011;32(8-9):4521-4527.
14. Sánchez-Pomales G, Santiago-Rodríguez L, Cabrera CR. DNA-Functionalized Carbon Nanotubes for Biosensing Applications. Journal of Nanoscience and Nanotechnology. 2009;9(4):2175-2188.
15. Zawrah MF, El-Kheshen AA, El-Shakour ZAA, El-Bassyouni GT, Hamzawy EMA. Boromullite/glass composites with improved thermal and electrical properties via maintaining the amorphous state of silica glass. Ceram Int. 2025;51(19):29762-29769.
16. Gradient Adsorption of Methylene Blue and Crystal Violet onto Compound Microporous Silica from Aqueous Medium. American Chemical Society (ACS).
17. Joni IM, Nulhakim L, Vanitha M, Panatarani C. Characteristics of crystalline silica (SiO_2) particles prepared by simple solution method using sodium silicate (Na_2SiO_3) precursor. Journal of Physics: Conference Series. 2018;1080:012006.
18. Zheng Y, Zheng Y, Ning R. Effects of nanoparticles SiO_2 on the performance of nanocomposites. Mater Lett. 2003;57(19):2940-2944.
19. Sibiya NP, Amo-Duodu G, Tetteh EK, Rathilal S. Model prediction of coagulation by magnetised rice starch for wastewater treatment using response surface methodology (RSM) with artificial neural network (ANN). Scientific African. 2022;17:e01282.
20. Daneshpayeh S, Ashenai Ghasemi F, Ghasemi I, Ayaz M. Predicting of mechanical properties of PP/LLDPE/TiO_2 nano-composites by response surface methodology. Composites Part B: Engineering. 2016;84:109-120.
21. Jesthi DK, Nayak RK. Influence of glass/carbon fiber stacking sequence on mechanical and three-body abrasive wear resistance of hybrid composites. Materials Research Express. 2020;7(1):015106.
22. Huang ZY, Lu SR, Yang ZY, Yu CH, Guo D. Studies on the Properties of Epoxy Resins Modified with Novel Liquid Crystalline Polyurethane. Advanced Materials Research. 2010;150-151:727-731.
23. Meure S, Wu D-Y, Furman SA. FTIR study of bonding between a thermoplastic healing agent and a mendable epoxy resin. Vib Spectrosc. 2010;52(1):10-15.
24. Sarafrazi M, Hamadanian M, Ghasemi AR. Optimize epoxy matrix with RSM/CCD method and influence of multi-wall carbon nanotube on mechanical properties of epoxy/polyurethane. Mech Mater. 2019;138:103154.
25. Zhang W, Fina A, Ferraro G, Yang R. FTIR and GCMS analysis of epoxy resin decomposition products feeding the flame during UL 94 standard flammability test. Application to the understanding of the blowing-out effect in epoxy/polyhedral silsesquioxane formulations. J Anal Appl Pyrolysis. 2018;135:271-280.
26. Sahmetlioglu E, Mart H, Yuruk H, Surme Y. Synthesis and characterization of oligosalicylaldehyde-based epoxy resins. Chemical Papers. 2006;60(1).
27. khezri T, Sharif M, Pourabas B. Polythiophene–graphene oxide doped epoxy resin nanocomposites with enhanced electrical, mechanical and thermal properties. RSC Advances. 2016;6(96):93680-93693.
28. Monteserín C, Blanco M, Aranzabe E, Aranzabe A, Laza JM, Larrañaga-Varga A, et al. Effects of Graphene Oxide and Chemically-Reduced Graphene Oxide on the Dynamic Mechanical Properties of Epoxy Amine Composites. Polymers. 2017;9(9):449.
29. Liu Z, Jiang Z, Fei B, Liu Xe. Thermal Decomposition Characteristics of Chinese Fir. BioResources. 2013;8(4).

30. Boursier Niutta C, Ciardiello R, Tridello A, Paolino DS. Epoxy and Bio-Based Epoxy Carbon Fiber Twill Composites: Comparison of the Quasi-Static Properties. Materials. 2023;16(4):1601.
31. Çeçen V, Sarikanat M, Yildiz H, Tavman IH. Comparison of mechanical properties of epoxy composites reinforced with stitched glass and carbon fabrics: Characterization of mechanical anisotropy in composites and investigation on the interaction between fiber and epoxy matrix. Polym Compos. 2008;29(8):840-853.
32. Kumar K, Goyat MS, Solanki A, Kumar A, Kant R, Ghosh PK. Improved mechanical performance and unique toughening mechanisms of UDM processed epoxy-SiO_2 nanocomposites. Polym Compos. 2021;42(11):6000-6009.
33. Liang M, Wong KL, Shanks R, Bansal V. Study of dielectric and mechanical properties of epoxy/SiO_2 nanocomposite prepared by different processing techniques. 2015 IEEE 11th International Conference on the Properties and Applications of Dielectric Materials (ICPADM); 2015/07: IEEE; 2015. p. 48-51.
34. Tsai S-N, Carolan D, Sprenger S, Taylor AC. Fracture and fatigue behaviour of carbon fibre composites with nanoparticle-sized fibres. Compos Struct. 2019;217:143-149.
35. Divya GS, Suresha B. Impact of nano-silicon dioxide on mechanical properties of carbon fabric reinforced epoxy composites. Materials Today: Proceedings. 2021;46:8999-9003.